Surface protected and modified iron based core-shell nanoparticles for biological applications†

Kanchana Somaskandan,[a] Teodor Veres,[b] Mereck Niewczas[c] and Benoit Simard*[a]

Received (in Gainesville, FL, USA) 6th August 2007, Accepted 5th October 2007
First published as an Advance Article on the web 25th October 2007
DOI: 10.1039/b711870h

Excellent quality superparamagnetic iron oxide coated iron nanoparticles were prepared *via* one pot synthesis with narrow size distribution. These particles were subsequently coated with Fe_xO_y, FePt or Pt shell to give long term protection to the highly reactive zero-valent iron core. Clear core-shell morphology was observed in the TEM images of Fe_xO_y and FePt coated particles and the magnetic properties suggested that these shells provided good protection to the core from oxidation, in particular iron oxide coated particles retained their magnetism for well over a year. FePt coated particles show superior magnetic properties to FePt particles alone and were found to be promising in biological applications. The magnetic studies further revealed that the saturation moments of the resultant particles were dependent on the type of shell used for encapsulation. Surface modifications of these particles were done with suitable hydrophilic ligands and they showed excellent stability and solubility in water and different buffer solutions which reveals the suitability of these nanoparticles for biomedical research.

Introduction

Iron is one of the most ubiquitous elements found on the earth's crust, with abundant possible uses. Both bulk and nano forms of iron have many unique properties that could be exploited for a variety of applications in engineering and medicine.[1–3] Nanosized iron magnets are currently receiving a great deal of attention in life science and health care research where they find use in tissue-specific drug delivery,[2] cell separation,[1] contrast enhancement agents in MRI,[3] and others. They are particularly useful in biomedical applications because other metallic, magnetic materials such as cobalt and nickel are quite toxic and may result in undesirable effects.[4,5] In order for nanoparticles to be used in biological tissues or within many bioassays they need to be small (less than 50 nm in diameter) and coated with suitable surface groups allowing the generation of a stable or colloidal aqueous solution under physiological conditions.[6,7] The use of superparamagnetic nanoparticles below 50 nm in diameter *in vivo* or within microfluidic channels is beneficial, because the small nanoparticles have very long sedimentation rates, and hence will not be excreted by the body, nor clog a microfluidic device.[8] For these reasons, iron and iron oxide particles are particularly attractive because they show superparamagnetism when particle diameters are $\leq$20 nm.[7,9]

In this regard iron oxides have been widely studied for biomedical research due to their low toxicity and excellent magnetic properties.[10–12] Many reports have been published on other magnetic alloy nanoparticles such as FePt[13–15] and FeCo[16] as they nicely complement iron oxides in terms of oxidation resistance and magnetism. However, all of the aforementioned nanocrystals are significantly weaker magnets in comparison to zero-valent iron nanoparticles. Therefore, if these materials could be replaced with pure iron, one would greatly enhance detection and manipulation capability. For example, the higher magnetic moment will yield nanoparticles with higher contrast capability in magnetic resonance experiments, resulting in more effective detection of cancer cells,[17,18] follow stem cell division to higher generation, or provide faster magnetic confinement of labeled biomarkers or cell in magnetic confinement assays.

A significant challenge in using iron instead of iron oxide is its extreme sensitivity to the presence of oxygen and water. Pure iron nanoparticles are generally stable under inert atmospheres in organic solvents, but yield mixtures of less magnetic iron oxides upon exposure to ambient conditions. Many different approaches have been used to protect this sensitive material from oxidation, including passivating the surface of the nanoparticles with different inorganic groups, such as iron oxide[19,20] and gold,[21–23] which offer superior passivation properties to their organic counterparts. However, it has been documented that non metallic surface layers negatively influence the desired magnetic properties.[24–26] As a result, iron nanoparticles are generally protected with metallic shells, with gold finding significant utility thanks to its relatively simple coating procedures and well known chemistry.[21–23] However, many of the reported metallic shells do not provide sufficient protection to the magnetic core because of non-uniform coating due to lattice mismatches and/or its roughness that allows oxygen to penetrate through the grain boundary, facilitating Fe oxidation. Furthermore, coating the magnetic particles

[a] *Steacie Institute for Molecular Sciences, National Research Council, Ottawa, Canada K1A 0R6. E-mail: Benoit.Simard@nrc-cnrc.gc.ca*
[b] *Industrial Materials Institute, National Research Council, Boucherville, Canada J4B 6Y4*
[c] *Department of Materials Science & Engineering, McMaster University, Hamilton, Canada L8S 4M1*
† Electronic supplementary information (ESI) available: Experimental details. See DOI: 10.1039/b711870h

with non magnetic gold will considerably decrease the magnetic moment by significantly contributing to the mass. However, a recent report from our group revealed that the stability and magnetism of Fe@Au nanoparticles can be significantly improved by laser assisted Au coating of Fe nanoparticles.[27] This investigation demonstrates the promise of this hybrid material, but also highlights how critical it is to thoroughly protect the highly reactive core in order to exploit its high magnetic moment for biological applications as mentioned earlier.

The Fe@Fe_xO_y[19,20] architectures have received interest from the research community because of structure compatibility between iron oxide and iron and the relative ease of preparation. One recent report[19] demonstrated the preparation of 35 nm Fe@Fe_xO_y nanoparticles using a hollow cathode sputtering cluster source followed by oxidation. These nanoparticles are stable against oxidation; however, their size is not in the superparamagnetic regime, which may pose some problems for use in some biological applications where the nanoparticles will readily aggregate and block channels or will be quickly eliminated from the body. Another report suggests that Fe@Fe_xO_y nanoparticles can be made by first preparing iron nanoparticles *via* colloidal wet chemistry followed by air exposure, which generates oxide layers.[20] However, there were no data on mass magnetization or the long term air stability of the final material. It has recently been suggested that iron nanoparticles synthesized *via* a colloidal route yield iron nanoparticles with an amorphous iron oxide coating[9,28] and that this 'natural oxide' coating cannot provide adequate protection to the reactive core, evidenced by the lowering of magnetic moment over time. Such 'native' iron oxide coated iron particles were prepared *via* reverse micelle reactions as well.[29]

Despite the difficulties in making stable iron nanoparticles, several groups have reported their synthesis. For example, a sonochemical method,[30] reduction of iron(II) and (III) salts,[31,32] decomposition of iron pentacarbonyl,[33–35] and chemical vapor deposition (CVD)[36] routes have been documented. However, particles prepared *via* the sonochemical route are generally amorphous and aggregated. A well known, general approach to produce high quality metal nanoparticles relies upon a mild reduction mediated by poly-alcohols. Yet the polyol reduction is not compatible with the generation of Fe nanoparticles because Fe salts must be catalyzed by acid or base. During the initial reduction, metal oxide nanoparticles are produced, which then are further reduced to zero-valent iron by a solid state reduction reaction that requires rigorous conditions and often results in sintering of particles. Another approach relies on the decomposition of iron carbonyl at high temperatures in the presence of surfactants and this procedure generates more uniform, crystalline particles. This popular metal carbonyl decomposition reaction can be carried out *via* either homogeneous or heterogeneous nucleation. The heterogeneous nucleation often utilizes Pt as a seed material upon which the iron is grown.[33] During the homogeneous preparation, the as-produced iron particles are readily oxidized possibly due to the carboxylate groups on the oleic acid surface ligand that was used to stabilize the particles. More recently, Sun *et al.* reported the synthesis of iron nanoparticles from iron carbonyl using oleylamine as the only surfactant in their preparation. The authors were able to produce Fe@Fe_xO_y core-shell structured particles in a single step[9] where magnetic moment reduction was observed over time most likely due to the porous nature of the iron oxide shell.

Therefore, our main goal is to obtain stable, highly magnetic material that retains its magnetic property over time. In order to achieve this, we surface protect the unstable iron nanoparticles with different shells, such as Fe_xO_y, FePt or Pt, *via* wet chemistry processes and herein we demonstrate their relative magnetic properties and some surface modification reactions to make the nanoparticles water-soluble and suitable for use in biological-based studies. In this study, iron oxide and FePt were chosen as shell materials because they are themselves magnetic and their crystal structures match that of iron very well. Although this may lead to a general reduction in mass magnetization due to a mass contribution from the shell, it will not be as significant as in the case of diamagnetic coating. Although, diamagnetic Pt was utilized because it should offer better oxidation resistance and therefore a thin shell or a couple of monolayers should be enough to provide good protection without a significant loss in magnetization. We show that intentional post coating of an iron core with a shell of Fe_xO_y and FePt provides better protection than the 'natural' iron oxide coating to the Fe core allowing further manipulation/modification of the nanoparticles for possible use in a biological labeling assay.

Experimental procedure

Materials

All reagents were used without further purification except hexane which was distilled over sodium. Dioctyl ether (99%), Pt(acetylacetonate)$_2$ (Pt(acac)$_2$, 97%), oleylamine (tech.), 1,2-hexadecanediol (tech., 90%), $Fe(CO)_5$ (99.999%), Fe(acac)$_3$ (99.9 + %), nonane (anhydrous 99 + %), dopamine hydrochloride, triethylene glycol 11-mercaptoundecyl ether ($HS(CH_2)_{11}(OCH_2CH_2)_3OH$, 95%), (1-mercaptoundec-11-yl)-hexa(ethylene glycol) ($HS(CH_2)_{11}(OCH_2CH_2)_6OH$), dimercaptosuccinic acid, Igepal (CO-520), and tetraethoxysilane (TEOS, 99.99%) were purchased from Aldrich. Oleic acid (elaidic acid, $\geq$ 97.0%) was received from Fluka.

Synthetic procedure

The synthetic routes are summarized in Scheme 1.

Fe nanoparticles (Fe@Fe_xO_y). Iron nanoparticles (solution **A**) were synthesized *via* a platinum seeded method according to a literature procedure with slight modifications.[33] Briefly, 10 mL of dioctyl ether, 4.0 mg of Pt(acac)$_2$, 0.9 mmol of oleic acid and/or 0.9 mmol of oleylamine and 0.6 mmol of 1,2-hexadecanediol were degassed for nearly 30 min and then heated to 80–100 °C under argon flow. 1.5 mmol of $Fe(CO)_5$ was injected into the hot solvent mixture and the temperature was increased. Black coloration was observed due to the nucleation of iron nanoparticles when the reaction temperature approached $\sim$ 200 °C. At 280 °C the solvent began to reflux, at which time the reaction was stopped and the solution was allowed to cool to room temperature. Another aliquot of

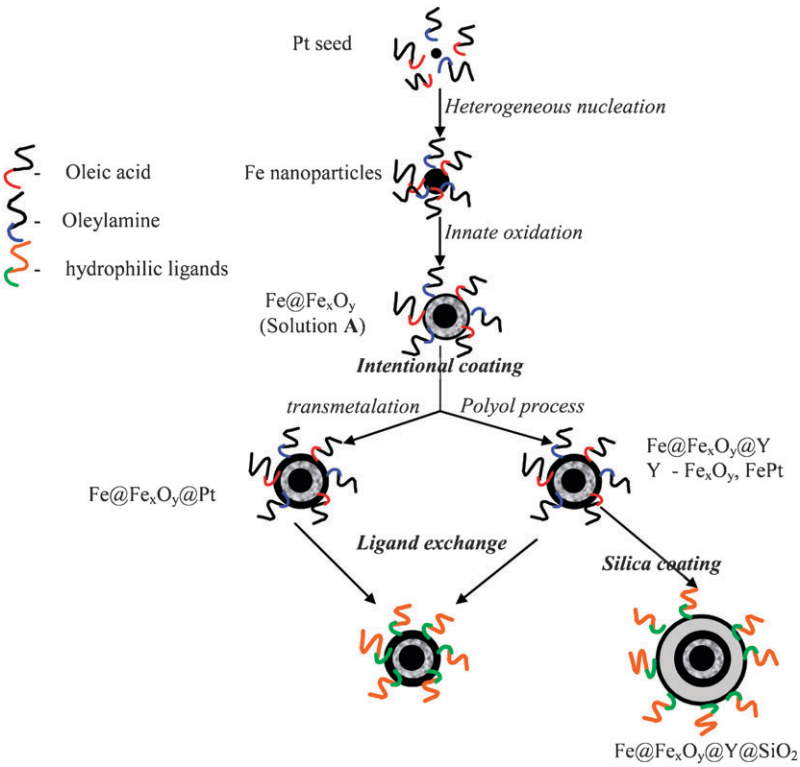

Scheme 1 Type of nanoparticles made at different stages of the preparation in the present study.

solvent was added to the mixture and the mixture was heated to ~ 100 °C. Another 7 mmol of $Fe(CO)_5$ were injected into the reaction mixture and the temperature was ramped up to refluxing point. Following 2 h of reflux, the reaction mixture was cooled to room temperature and the particles were isolated in a nitrogen dry box with ethanol and hexane. The isolated material was redispersed in hexane and kept in the dry box prior to intentional coating. The particles prepared in this step will be denoted as **Fe**@Fe_xO_y hereafter.

Fe_xO_y and FePt coating. Iron oxide or Fe_xO_y (*i.e.* Fe_xO_y may contain Fe_3O_4 and/or Fe_2O_3) coating was performed *via* a polyol process as described here. 0.7 mmol of $Fe(acac)_3$, 3.3 mmol of 1,2-hexadecanediol, 0.5 mmol of oleic acid, 0.5 mmol of oleylamine were taken in 10 mL of dioctyl ether and degassed for 20 min. Then the mixture was heated to 60 °C under Ar and ~ 5–7 mL of hexane solution of Fe nanoparticles **A** were injected. The reaction flask was kept open under heavy Ar flow at ~ 100 °C for up to 15 min to remove any hexane from the reaction mixture. Then, the resultant mixture was refluxed under Ar for 2 h to yield a brownish black solution. The resultant mixture was allowed to cool to room temperature and the isolation and purification were done in air with hexane–ethanol solvent–antisolvent pair. Purified particles were dried under nitrogen and used for the next step.

In addition to the above reagents, 0.25 mmol of $Pt(acac)_2$ was used with 0.5 mmol of $Fe(acac)_3$ to grow FePt shell on Fe nanoparticles.

Pt coating. 0.1 mmol of $Pt(acac)_2$ was placed in 15 mL of nonane with 0.1 mmol of dodecyl isonitrile[37] as the stabilizing agent. To the mixture, 0.2 mmol of already prepared dry Fe nanoparticles (precipitated from solution **A**) were added as seeds. The reaction proceeded at 150 °C for about 6 h.

Surface modification of particles

Fe@Fe_xO_y@Fe_xO_y coated particles. Surface ligand exchange of iron oxide coated particles was done with dopamine hydrochloride and dopamine PEG ligands. In both cases the weight ratio between the particles and ligand was kept to 1 : 1.5–2.

a. Dopamine exchange

An amount of 25 mg of dry particles was dissolved in 3 mL of anhydrous toluene. Separately, about 40 mg of dopamine hydrochloride were dissolved in 2 mL of methanol. These two solutions were mixed and stirred at 40 °C under Ar for ~ 48 h. The particles were isolated from the solution and washed thoroughly with methanol to remove any excess ligands. These particles were readily soluble in water.

b. Dopamine PEG exchange

Both particles and dopamine-PEG (prepared in the laboratory according to a literature procedure,[38] see ESI†) ligand were dissolved in ~ 10 mL of dichloromethane and vortex mixed at room temperature for ~ 48 h. Diethyl ether was added to the resultant mixture and the particles were isolated by centrifugation.

c. Silica coating

Silica coating of iron oxide coated iron particles was done using a reverse microemulsion technique reported by Korgel *et al.* recently[39] with slight modifications. Briefly, 3.2 mg of dried particles were dissolved in 3.2 mL of hexane and this was added to a mixture of 22 mL of cyclohexane and 1.06 mL of Igepal under vigorous stirring. Slowly and dropwise, 0.26 mL of 28% NH_4OH was added into the reaction mixture while

sonicating in the bath. Then, the mixture was stirred for 5–10 min, and 90 μL of TEOS were added. The resulting emulsion was stirred or shaken for ~ 72 h to yield a uniform silica coating around the superparamagnetic nanoparticles. Particles were dispersed in methanol and excess hexane was added to precipitate them. Finally, the particles were purified using ethanol.

Fe@Fe$_x$O$_y$@FePt and Fe@Fe$_x$O$_y$@Pt coated particles. Surface exchange of these particles was done using several thiol ligands as Pt has good affinity to sulfur. The ligands mainly used for this purpose were dimercaptosuccinic acid (DMSA), hexa(ethylene glycol) mono-11-mercaptoundecyl ether (HSPEG-1) and triethylene glycol 11-mercaptoundecyl ether (HSPEG-2). Particles were dispersed in toluene and the ligands were dissolved in DMF (for DMSA), methanol or added directly (for HSPEG 1 and HSPEG 2) into the toluene solution. The final solutions were vortex mixed for ~ 40 h. In the case of HSPEG ligands, the solutions were heated to ~ 40 °C while stirring.

Silica coating of the **Fe**@Fe$_x$O$_y$@**FePt** particles was carried out with an approach similar to that described for the **Fe**@Fe$_x$O$_y$@**Fe$_x$O$_y$** particles.

Characterization

Initial structural characterization of the synthesized materials was done using a Bruker AXS X-ray diffractometer operated at 40 kV and 40 mA with Cu as anode. Patterns were collected within the 2Θ range of 10° to 70°. TEM images were taken using a Philips CM20 FEG instrument operating at 200 kV with an EDS (energy dispersive spectroscopy) attachment. Magnetic characterization of the particles was done with Quantum design PPMS-9 and PPMS model 6000 magnetometers. Field cooled (FC) and zero field cooled (ZFC) data were collected from 10 K to 350 K at the applied field of 50 Oe. Quantitative analyses were done with ICP-AES.

Results and discussion

Iron nanoparticles were prepared *via* a high temperature colloidal route and were intentionally coated with different metallic shells to protect the highly reactive core. The heterogeneous nucleation route was employed for the preparation of Fe nanoparticles as it was shown in the literature that oxidation was minimal in this route.[33] During the synthesis, platinum seeds were initially produced from Pt(acac)$_2$ in dioctyl ether using oleic acid and/or oleylamine as passivating agents. Heterogeneous growth of Fe nanoparticles was continued from the thermal decomposition of Fe(CO)$_5$ over already formed Pt seeds at high temperature. Intentional coating of the as prepared and isolated Fe nanoparticles was performed with Fe$_x$O$_y$, FePt, and Pt *via* polyol reduction (for Fe$_x$O$_y$ and FePt shells) and redox active transmetalation (for Pt coating).[40] But, Pt coating was not successful due to the inherent iron oxide layer found on the Fe nanoparticles.

Powder X-ray diffraction patterns for the Fe nanoparticles formed in the first step did not show any distinct features but broad peaks centered around 30 and 43° (Fig. 1a). Generally, particles prepared using this route yield amorphous Fe nanoparticles that do not give any characteristic features in XRD. This indicated that the particles were small and did not have long range crystalline order to give peaks in the XRD pattern. However, as the broad peak centered around 2Θ = 43° extends up to 45°, where a peak for α-Fe is generally observed, one can argue that Fe nanoparticles were indeed prepared during the synthesis. Additionally, the humps overlap the 2Θ region of iron oxide as well. This suggests that some degree of oxidation had occurred in the sample and the oxide formed had poor crystallinity. This observation differs from Vargas *et al.*'s work, who reported a polycrystalline iron oxide shell upon exposure of Fe nanoparticles to air.[20] This oxide formation can be further evidenced by the TEM images where clear core-shell morphology at relatively higher magnifications was observed (Fig. 2a).

This oxidation may be due to either exposure of the particles to air or innate iron oxide formation during the reaction. It also has been reported in the literature that when excess Fe(CO)$_5$ was used in FePt synthesis, a Fe$_3$O$_4$ shell was observed on the particles upon brief air exposure.[41] Because our synthetic protocols and isolation were done strictly under inert conditions, the oxidation would have happened either during the transport of sample to PXRD and TEM measurements or due to the trace amounts of accidental oxygen

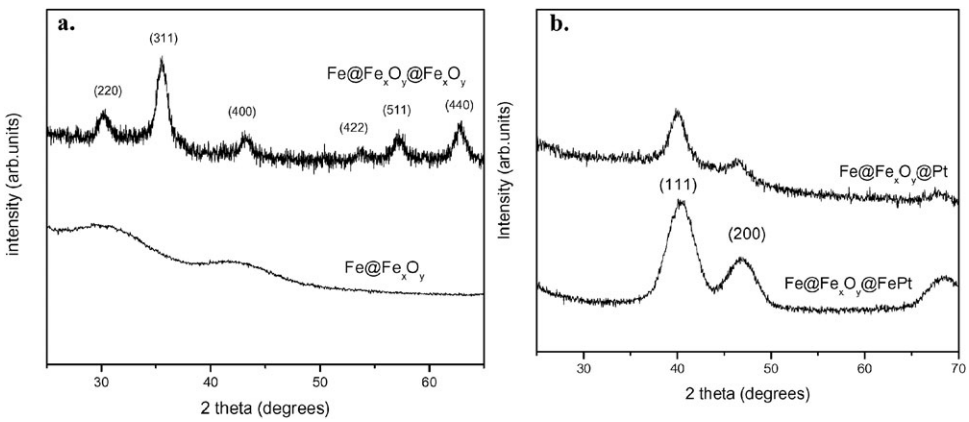

Fig. 1 PXRD patterns of (a) **Fe**@Fe$_x$O$_y$ (bottom) and **Fe**@Fe$_x$O$_y$@**Fe$_x$O$_y$** (top) showing peaks for Fe$_3$O$_4$ and (b) **Fe**@Fe$_x$O$_y$@**Pt** and **Fe**@Fe$_x$O$_y$@**FePt** nanoparticles showing peaks for Pt/FePt.

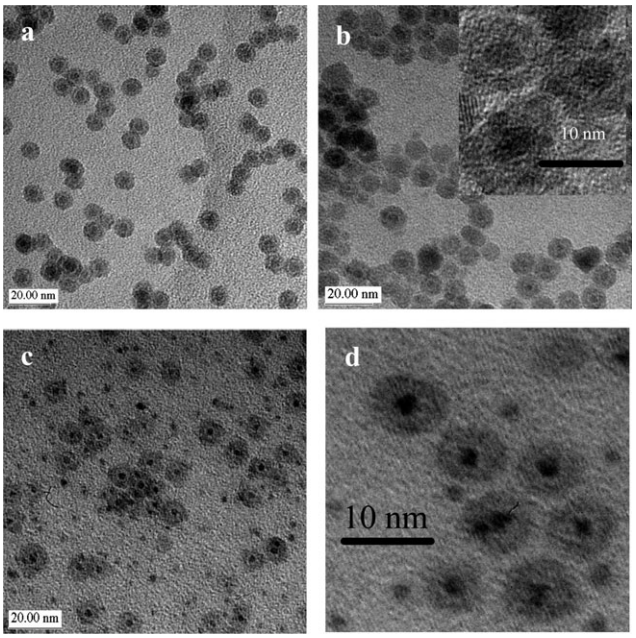

Fig. 2 TEM images of (a) as prepared **Fe**@Fe_xO_y, (b) **Fe**@Fe_xO_y-@**Fe_xO_y**. Inset shows the high magnification image of (b). **Fe**@Fe_xO_y@**FePt** nanoparticles under low (c) and high (d) magnifications.

present, especially during the isolation process. Moreover, structural characterization such as TEM and XRD of this material suggested that both the core and the shell of as-formed **Fe**@Fe_xO_y particles were not highly crystalline, as evidenced by the lack of distinct peaks or fringes observed during these measurements. Presence of Fe(0) was further confirmed by XPS characterization of the particles, which revealed the existence of both zero-valent Fe and oxidized Fe(II) and (III) in the spectrum. Interestingly, this amorphous iron oxide shell layer was able to protect the Fe(0) core from oxidation for nearly a month. TEM images of these particles after storage in air for 18 h (Fig. S1 a and b in ESI†) suggested that no reduction in core size (3.93 ± 0.55 nm *vs.* 4.25 ± 0.57 nm) was observed; however, the iron core was oxidized to Fe_xO_y following a month of air exposure, as evidenced by the disappearance of the core-shell architecture in some of the nanoparticles in the TEM images. Sun *et al.* reported recently that the magnetic moment of Fe nanoparticles with an amorphous iron oxide shell decreased significantly after a day of exposure to air.[9] This revealed that the amorphous shells around the Fe nanoparticles were quite porous, which allowed oxygen to react with the core and reduced the magnetic moment. This is the case for our samples after a prolonged air exposure. However, the **Fe**@Fe_xO_y nanoparticles that we prepared are significantly more stable than those previously reported in terms of oxidation resistance.

Despite the fact that the **Fe**@Fe_xO_y nanoparticles show significantly better oxidation resistance, we were interested in developing a means by which a highly crystalline shell could be grown on the nanoparticle in order to improve both the magnetic properties and long term stability of the particles. PXRD patterns of particles after intentional coating of Fe_xO_y and FePt are shown in Fig. 1a and b, respectively. Particles with a Fe_xO_y shell gave crystalline peaks corresponding to the Fe_3O_4 crystalline phase whereas particles that were coated with FePt and Pt showed clear peaks indicative of FePt and Pt (both diffract at similar 2Θ values), respectively (Fig. 1b).

Table 1 Particle sizes obtained from TEM images before and after coating with different shells

Shell type	Particle size before coating **Fe**@Fe_xO_y/nm	Particle size after coating **Fe**@Fe_xO_y@shell/nm
Fe_xO_y	8.01 ± 0.74 (±9%)	10.22 ± 1.20 (±11%)
FePt	7.35 ± 0.89 (±12%)	8.20 ± 0.66 (±8%)
Pt	7.61 ± 0.94 (±12%)	6.24 ± 1.11 (±18%)

TEM was a valuable characterization tool for these unique nanoparticles. For example, TEM images of the particles after intentional coating of a second shell confirmed that the core-shell morphology was retained in the case of Fe_xO_y and FePt (Fig. 2b and c) shells. Additionally, the FePt coating process yielded free FePt nanoparticles (Fig. 2c and d). However, during iron oxide coating core dissolution or oxidation was observed in some of the particles. In order to demonstrate whether there is any size increment due to shell growth, particle sizes were measured before and after the intentional growth of the second shell (Table 1). For example, for iron oxide coated particles, the overall size of the particles (*i.e.* **Fe**@Fe_xO_y) synthesized in the first step was 8 nm and after the coating the size went up to 10 nm. This clear size difference indicates the presence of additional material around the particles. The TEM image of FePt coated particles (Fig. 2c and d) revealed that some small particles did not possess core-shell morphology. These smaller (1.85 ± 0.27 nm) nanoparticles are most likely individual FePt particles formed during the synthesis. Furthermore, the size of the core (1.65 ± 0.22 nm) is somewhat similar to the size of newly nucleated particles and no significant increase in the overall size of the nanoparticles possessing core-shell morphology (Table 1 gives the size of only coated particles) is observed. However, the EDS analysis (Table 2) on **Fe**@Fe_xO_y@**FePt** particles showed the presence of both Fe and Pt in the spectrum, providing additional evidence supporting the formation of an FePt shell, which may be very thin in this case. Unfortunately, coating the **Fe**@Fe_xO_y nanoparticles with Pt did not show any significant contrast difference between the core and the shell despite the evidence of Pt existence in PXRD and EDS results. In order to rule out that the Pt found in EDS analysis was not from the Pt seeds used in the synthesis, we performed EDS analysis on both the iron oxide coated and Pt coated iron nanoparticles. These quantitative analyses showed that the ratio between Fe, Pt, and O was 2 : 0 : 5 and 5 : 1 : 9 in Fe_xO_y and Pt coated particles, respectively. This could be attributed to either a very thin layer of coating or formation of individual Pt

Table 2 EDS analysis results of coated particles

	Atomic %		
Sample	Fe	Pt	O
Fe@Fe_xO_y@**Fe_xO_y**	28.12	ND	71.87
Fe@Fe_xO_y@**FePt**	26.88	6.11	67.04
Fe@Fe_xO_y@**Pt**	34.31	6.49	59.18

ND – Not Detected.

nanoparticles in the reaction mixture since there was no size change after Pt coating. It is worthwhile mentioning here that a redox active transmetalation process, *i.e.* reduction of Pt(II) on the surface of Fe(0), was our aim to have Pt around Fe. Since the initial iron particles have an iron oxide shell, there wouldn't be any reduced metal on the surface to give an electron for Pt(II) reduction. Furthermore, the broad size distribution (± 18%) observed in this sample supports the individual Pt nanoparticle formation during the coating procedure. In order to eliminate or minimize the oxide layer, shelling reactions were attempted in the same pot in which Fe nanoparticles were synthesized. However, these reactions too did not yield the required morphology.

While synthesized iron nanoparticles could be easily isolated from the reaction mixture using an external magnet, the magnetic response of the coated particles showed a relatively low and varied response depending on the encapsulated material. For example, Fe_3O_4 coated particles showed a very good response over a FePt shell and particles with a Pt shell showed the least response. These observations can be attributed to the less magnetic or non magnetic second shell that masks the magnetic property of iron nanoparticles. This qualitative analysis was further confirmed by systematic measurements of their magnetic properties.

According to these measurements all coated and uncoated particles showed superparamagnetism with a blocking temperature characteristic for given particles. The plots of magnetization per gram of samples *vs.* applied magnetic field are given in Fig. 3 for uncoated and coated particles. The saturation magnetization of **Fe**@Fe_xO_y nanoparticles at 300 K showed the highest value, 51 emu g^{-1} of sample. When the magnetization is expressed with respect to iron itself (*i.e.* emu per gram of Fe), which was obtained using ICP-AES analyses, these nanoparticles showed 127 emu g^{-1}, which is indeed a very good value for iron nanoparticles prepared *via* a colloidal route. The reduced moment, which is less than that of bulk Fe value: 218 emu g^{-1}, suggests that the particles lack long range

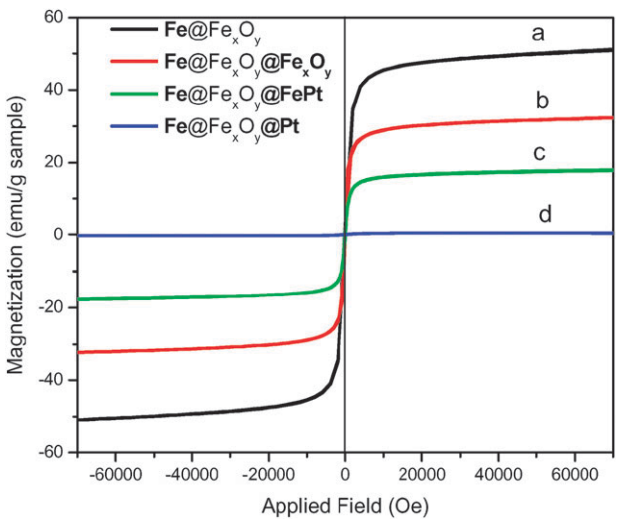

Fig. 3 *M vs. H* measurements of (a) as prepared **Fe**@Fe_xO_y, and intentionally coated with (b) **Fe_xO_y**, (c) **FePt**, and (d) **Pt** shells at 300 K.

crystalline order and are terminated with a significant amount of iron oxide. This can be further supported by the volume fraction of metallic iron determined from the TEM data, which revealed that the particles contained ~ 8% of iron by volume. When this was translated to the quantitative amount of iron obtained from ICP-AES analysis, nearly 23% of the mass comes from zero-valent iron. It was reported in the literature that amorphous Fe nanoparticles prepared *via* a sonochemical method showed the saturation magnetization value of 156 emu g^{-1}.[30] However, these particles formed agglomerates and their size was as big as 30 nm. In the present study, although freshly made iron particles had shown an excellent magnetic response, the semi-porous iron oxide shell permits oxidation, which transforms the core to iron oxide over time, resulting in a reduction in magnetization. It is necessary to mention here that during this study the time interval between the synthesis and magnetic measurements was usually from several days to a few weeks. Another key factor contributing to the lower magnetic moments is the strength of interaction between the surfactant(s) and the particle. This has been studied on iron nanoparticles prepared using different surfactants where lowering of saturation magnetization was observed due to strongly interacting surfactants.[35] For example, particles coated with alcohols (85 emu g^{-1} Fe) and carboxylic acids (55 emu g^{-1} Fe) showed an order of magnitude higher mass magnetization than strongly interacting phosphonic acids (5 emu g^{-1} Fe) with the same number of carbon atoms. Although the mass of Fe in the sample can be obtained from quantitative analysis, it is quite difficult to determine the exact amount of surface groups present in the sample. This contributes additional error in the mass magnetization calculation in magnetic nanoparticles. However, in the present study, attempts to make Fe particles with less interacting surfactants, such as acetylacetone, yielded particles that were immediately precipitated out from the solutions. A similar observation was reported by Huber *et al.* when acetylacetone was used as passivation agent to make iron nanoparticles.[42] We observed that the mass magnetization calculated from magnetization measurements and quantitative analysis for **Fe**@Fe_xO_y@**Fe_xO_y** nanoparticles was as high as 62 emu g^{-1} Fe at 300 K. Considering the effects already mentioned the saturation moment calculated for **Fe**@Fe_xO_y@**Fe_xO_y** nanoparticles was consistent with the additional iron oxide coating around the particles. However, this M_s value can be retained for a longer period due to the stable protective shell. As a result, these materials will be potential candidates for several biomedical and technological applications. Nevertheless, a significant improvement in magnetism can be achieved by making bigger and/or more crystalline Fe nanoparticles. Our attempt to synthesize such particles using a different Fe precursor, namely $Fe_2(CO)_9$, yielded nearly 15 nm particles, but they were iron oxide nanocrystals. Interestingly, FePt coated particles showed a significantly high M_s value of 20 emu g^{-1} of sample and no further quantitative analysis was carried out on these particles. Generally, particles synthesized by a similar wet-chemistry method consist of ~ 30–50% of surfactants by weight. It was shown in a recent report that nearly 50–66% of surfactant mass remained on an iron nanoparticle surface even after several washings.[33] In the

present work particles were washed only two or three times in order to facilitate post-synthetic manipulation and this would have left behind a good proportion of surfactant in the samples. According to ICP-AES analysis, as synthesized **Fe**@Fe_xO_y nanoparticles generally contained 40–55% of iron by weight. Therefore, in order to get a rough estimate of the magnetic moment of FePt coated particles, we assume that the amount of surfactant present is about 50%. This amount leads to an estimated moment value of 40 emu per g of Fe, which is an excellent value for the saturation moment for FePt coated particles prepared under present conditions. Since FePt is versatile and can be functionalized relatively easily, this mass magnetization value is good enough for many biological applications. Further, it is an excellent alternative to Au and uses similar chemistries but is better in terms of magnetism. These FePt coated Fe nanoparticles show excellent promise for current and future biological applications, and it is shown in the next section that they can be surface exchanged to yield water soluble, functionalized particles. Unfortunately, Pt coated iron nanoparticles lost a significant amount of their magnetism and showed a poor value of M_s of 2 emu per g of sample. As was explained before, if a Pt shell was not formed around the core, the zero-valent iron would have completely oxidized to amorphous iron oxide and/or hydroxides. These compounds drastically affect the magnetic properties. Therefore, one of the reasons for this poor M_s value could be complete oxidation of the core.

Surface ligands of the coated particles were place exchanged using suitable hydrophilic groups to facilitate the water solubility of the particles. This step is important in order to use these materials in biological tests after proper surface modifications. Hydrophilic groups such as dopamine hydrochloride and dopamine-PEG were used to exchange the surface of iron oxide coated particles as dopamine was shown to be a better anchor for a particle surface with iron oxide.[43] Although thiolated organic molecules are good surface exchange groups for noble metals, their utility was not shown for iron oxide surfaces. However, reports have demonstrated that organic sulfur compounds are versatile exchange groups for Pt containing nanomaterials.[38,44,45] In this regard thiolated polyethylene glycols and dimercaptosuccinic acid were utilized for ligand exchange on FePt and Pt coated particles.

Surface exchanged iron oxide particles showed excellent solubility in polar solvents and buffers and quite narrow size distribution without any significant aggregation during the exchange process. They possessed very good colloidal stability over time both in water and buffers (Fig. S2 a and b, ESI†). Their stability was tested in different pH buffers since our aim is to use these particles in biological experiments, such as studies on blood and urine. In this regard, the stability was monitored in pH 6 and 7.6 buffer solutions. In order to mimic blood, 0.3 M salt was added to a pH 7.6 buffer. The solubility of the exchanged particles in both buffers was very good (Fig. S3 a and b, ESI†) and particles dissolved in a pH 6 buffer showed excellent stability over time (several weeks) in comparison to others. Preliminary magnetic studies showed that these exchanged particles retained the magnetism very well over time.

While this manuscript was in preparation, Shultz *et al.* reported the reactive nature of dopamine as a surface functionalization ligand on iron oxide nanoparticles.[46] It was shown that the oxidized dopamine undergoes a rearrangement and significantly degrades the nanoparticles. They further reported that the product formed during the transformation is blue color semiquinone, which is cytotoxic and therefore iron oxide particles surface exchanged with dopamine may not be useful in biomedical applications. However, in our study, although we observed the initial blue coloration in the aqueous solution we did not see any green precipitation, which was attributed by Shultz *et al.* to a mixture of iron oxide and iron(II) hydroxide formed over time. Instead, the initial blue coloration disappeared after a day and the solution became clear brownish black similar to unexchanged particles. Additionally, we did not observe any band at 400 nm due to complete oxidation of dopamine to dopaminochrome[46] in the UV spectrum (Fig. S4, ESI†). The absence of the band in our studies may be due to spontaneous, light induced transformation of dopaminochrome to UV-transparent leucodopaminochrome.

Good water solubility was also observed with exchanged FePt and Pt coated particles with DMSA showing excellent and stable solution with MES buffer. Following deprotonation of the acid with a drop of 0.1 M NaOH, aqueous solutions of DMSA exchanged particles were readily soluble. Although mercapto PEG exchanged particles possessed good solubility in water, cloudiness or some extent of sedimentation was observed after a day or two in those vials. The cloudiness observed may be due to the amphiphilic nature of the PEG ligand. However, the supernatant remains dark brown color weeks after exchange, which suggests that the exchange was successful and the PEG moieties remain anchored to the FePt surface. The stability of the particles could be improved by

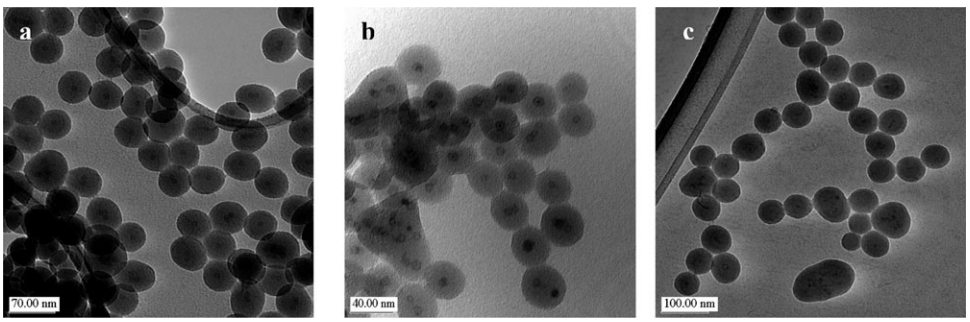

Fig. 4 TEM images of silica coated (a) **Fe**@Fe_xO_y, (b) **Fe**@Fe_xO_y@**Fe_xO_y**, and (c) **Fe**@Fe_xO_y@**FePt** nanoparticles.

Table 3 Stability and mass magnetization of different materials prepared in the study

Material	Stability	Mass magnetization emu g^{-1} Fe
Fe@Fe_xO_y	A few weeks to a month	127
Fe@Fe_xO_y@**Fe_xO_y**	Several months to a year	62
Fe@Fe_xO_y@**FePt**	Several months to a year	~ 40

using ammonium-terminated or carboxylate-terminated PEG-thiol groups.[38] The water solubility and stability results obtained with surface modified core-shell magnetic particles show promise for biological applications. Water soluble **Fe**@Fe_xO_y@**Fe_xO_y** particles are presently being utilized in biological experiments and the results arising from this work will be published separately.

The other type of surface modification is constructing a bio-friendly silica shell around the superparamagnetic nanoparticles. Silica encapsulation of iron oxide and iron–platinum coated particles showed clear core-shell morphology with the magnetic particles centered in the more regular silica nanobeads (Fig. 4a–c). In fact, the core-shell morphology of **Fe**@Fe_xO_y@**Fe_xO_y** particles could be seen clearly inside the silica matrix. The shell thicknesses were in the range of 10–16 nm with the total particle size of 30–40 nm. Further, they showed very good solubility in water and other polar solvents such as methanol and ethanol. Interestingly, when **Fe**@Fe_xO_y-@**Fe_xO_y** particles kept in the ambient conditions over a year were used for silica coating, clear core-shell morphology of Fe/Fe_xO_y was still observed within the silica beads during TEM imaging (Fig. S5, ESI†). This reveals that the crystalline iron oxide coating acts as an excellent sealant in protecting highly reactive iron nanoparticles. Additionally, it was possible to construct a silica shell around the **Fe**@Fe_xO_y particles. Studies which explore using **Fe**@Fe_xO_y@**SiO_2** as magnetic capture probes in a biological environment are under way. It is worthwhile mentioning here that in order to make a multi-functional material to be used in biological detection our laboratory is involved in making dye doped silica nanoparticles. These materials have a basic structure similar to the silica coated superparamagnetic nanoparticles explained here with an additional silica coating that is doped with dye molecules.[47] They are excellent probes for rapid diagnostics, photo-therapies, and imaging technologies.

Conclusion

Nearly monodispersed, superior quality **Fe**@Fe_xO_y core-shell nanoparticles were synthesized using high temperature wet chemistry with usual surfactant(s) *via* a single step. Although it was possible to protect these highly magnetic particles for a month, they were further passivated with additional shells and/or groups to provide enhanced stability and amenability. Among the shell materials used in the study, iron oxide coated Fe nanoparticles retain their magnetic properties for well over one year and appear promising for biological applications where a higher magnetic moment is required (Table 3). Further, Fe nanoparticles encapsulated with a FePt shell appear to have improved magnetic properties over pure FePt nanoparticles and hence these are useful substitutes for iron oxide and complementary to gold nanoparticles. Currently, conditions are being optimized to get larger, more crystalline Fe nanoparticles using $Fe(CO)_5$ as Fe precursor to further improve the magnetization. To make the highly magnetic iron oxide and iron–platinum coated Fe nanoparticles useful for biological purposes surface ligands were exchanged with suitable hydrophilic groups and coated with silica. Their excellent stability in aqueous and different pH solutions was also demonstrated.

Acknowledgements

We extend our thanks to Catherine Bibby of Natural Resources Canada for assisting in taking TEM images; David Kingston of the Institute for Chemical Process and Environmental Technology for the XPS measurements; and Christine Scriver of the Institute for National Measurement Standards, National Research Council Canada for analysing our samples using the ICP-AES technique. Our sincere thanks to Dr Arnold Kell for useful discussions and suggestions while preparing this manuscript. We would like to acknowledge Genome Canada and Genome Quebec for their generous funding of this work.

References

1 H. H. Yang, S. Q. Zhang, X. L. Chen, Z. X. Zhuang, J. G. Xu and X. R. Wang, *Anal. Chem.*, 2004, **76**, 1316–1321.
2 P. K. Gupta and C. T. Hung, *Life Sci.*, 1989, **44**, 175–186.
3 R. Weissleder, A. Bogdanov, E. A. Neuwelt and M. Papisov, *Adv. Drug Delivery Rev.*, 1995, **16**, 321–334.
4 P. Tartaj, M. P. Morales, V.-V. Verdaguer, T.-G. Carreno and C. J. Serna, *J. Phys. D: Appl. Phys.*, 2003, **36**, R182–R197.
5 K. Wormuth, *J. Colloid Interface Sci.*, 2001, **241**, 366–377.
6 M. A. Willard, L. K. Kurihara, E. E. Carpenter, S. Calvin and V. G. Harris, *Int. Mater. Rev.*, 2004, **49**, 125–170.
7 Y. P. He, S. Q. Wang, C. R. Li, Y. M. Miao, Z. Y. Wu and B. S. Zou, *J. Phys. D: Appl. Phys.*, 2005, **38**, 1342–1350.
8 C. Alexiou, R. Jurgons, C. Seliger and H. Iro, *J. Nanosci. Nanotechnol.*, 2006, **6**, 2762–2768.
9 S. Peng, C. Wang, J. Xie and S. Sun, *J. Am. Chem. Soc.*, 2006, **128**, 10676–10677.
10 T. Hyeon, S. S. Lee, J. Park, Y. Chung and H. B. Na, *J. Am. Chem. Soc.*, 2001, **123**, 12798–12801.
11 S. Qu, H. Yang, D. Ren, S. Kan, G. Zou, D. Li and M. Li, *J. Colloid Interface Sci.*, 1999, **215**, 190–192.
12 J. Park, E. Lee, N.-M. Hwang, M. Kang, S. C. Kim, Y. Hwang, J.-G. Park, H.-J. Noh, J.-Y. Kim, J.-H. Park and T. Hyeon, *Angew. Chem., Int. Ed.*, 2005, **44**, 2872–2877.
13 S. Sun, C. B. Murray, D. Weller, L. Folks and A. Moser, *Science*, 2000, **287**, 1989–1992.
14 S. Sun, E. E. Fullerton, D. Weller and C. B. Murray, *IEEE Trans. Magn.*, 2001, **37**, 1239–1243.
15 B. Stahl, N. S. Gajbhiye, G. Wilde, D. Kramer, J. Ellrich, M. Ghafari, H. Hahn, H. Gleiter, J. Weissmuller, R. Wurchum and P. Scholossmacher, *Adv. Mater.*, 2002, **14**, 24–27.
16 C. W. Kim, Y. H. Kim, H. G. Cha, H. W. Kwon and Y. S. Kang, *J. Phys. Chem. B*, 2006, **110**, 24418–24423.
17 Y.-M. Huh, Y.-W. Jun, H.-T. Song, S. Kim, J.-S. Choi, J.-H. Lee, S. Yoon, K.-S. Kim, J.-S. Shin, J.-S. Suh and J. Cheon, *J. Am. Chem. Soc.*, 2005, **127**, 12387–12391.
18 H. Lee, E. Lee, D. K. Kim, N. K. Jang, Y. Y. Jeong and S. Jon, *J. Am. Chem. Soc.*, 2006, **128**, 7383–7389.
19 L. T. Kuhn, A. Bojesan, L. Timmermann, M. M. Nielson and S. Morup, *J. Phys.: Condens. Matter*, 2002, **14**, 13551–13567.
20 J. M. Vargas, L. M. Socolovsky, G. F. Goya, M. Knobel and D. Zanchet, *IEEE Trans. Magn.*, 2003, **39**, 2681–2683.

21 W. Zhou, A. Kumbhar, J. Weimann, J. Fang, E. E. Carpenter and C. J. O'Connor, *J. Solid State Chem.*, 2001, **159**, 26–31.
22 S.-J. Cho, J.-C. Idrobo, J. Olamit, K. Liu, N. D. Browning and S. M. Kauzlarich, *Chem. Mater.*, 2005, **17**, 3181–3186.
23 S.-J. Cho, B. R. Jarrett, A. Y. Louie and S. M. Kauzlarich, *Nanotechnology*, 2006, **17**, 640–644.
24 C. Pathmamanoharan and A. P. Philipse, *J. Colloid Interface Sci.*, 1998, **205**, 340–353.
25 M. Klotz, A. Ayral, C. Guizard, C. Ménager and V. Cabuil, *J. Colloid Interface Sci.*, 1999, **220**, 357–361.
26 D. V. Szabo and D. Vollath, *Adv. Mater.*, 1999, **11**, 1313–1316.
27 J. Zhang, M. Post, T. Veres and B. Simard, *J. Phys. Chem. B*, 2006, **110**, 7122–7128.
28 H. Shao, H. Lee, Y. Huang, I. Y. Ko and C. Kim, *IEEE Trans. Magn.*, 2005, **41**, 3388–3390.
29 E. E. Carpenter, S. Calvin, R. M. Stroud and V. G. Harris, *Chem. Mater.*, 2003, **15**, 3245–3246.
30 M. W. Grinstaff, M. B. Salamon and K. S. Suslick, *Phys. Rev. B: Condens. Matter Mater. Phys.* , 1993, **48**, 269–273.
31 J. P. Wilcoxon and P. P. Provencio, *J. Phys. Chem. B*, 1999, **103**, 9809–9812.
32 H. Bonnemann, W. Brijoux and T. Joussen, *Angew. Chem., Int. Ed. Engl.*, 1990, **29**, 273–275.
33 D. Farrel, S. A. Majetich and J. P. Wilcoxon, *J. Phys. Chem. B*, 2003, **107**, 11022–11030.
34 G. Kataby, M. Cojocaru, R. Prozorov and A. Gedanken, *Langmuir*, 1999, **15**, 1703–1708.
35 G. Kataby, Y. Koltypin, A. Ulman, I. Felner and A. Gedanken, *Appl. Surf. Sci.*, 2002, **201**, 191–195.
36 F. Zaera, *J. Vac. Sci. Technol., A*, 1989, **7**, 640–645.
37 W. Weber and G. W. Gokel, *Tetrahedron Lett.*, 1972, 1637–1640.
38 R. Hong, N. O. Fischer, T. Emrick and V. M. Rotello, *Chem. Mater.*, 2005, **17**, 4617–4621.
39 D. C. Lee, F. V. Mikulec, J. M. Pelaez, B. Koo and B. A. Korgel, *J. Phys. Chem. B*, 2006, **110**, 11160–11166.
40 W.-R. Lee, M. G. Kim, J.-R. Choi, J. Park, S. J. Ko, S. J. Oh and J. Cheon, *J. Am. Chem. Soc.*, 2005, **127**, 16090–16097.
41 M. Chen, J. P. Liu and S. H. Sun, *J. Am. Chem. Soc.*, 2004, **126**, 8394–8395.
42 D. L. Huber, J. E. Martin, E. L. Venturini, P. P. Provencio and R. J. Patel, *J. Magn. Magn. Mater.*, 2004, **278**, 311–316.
43 C. Xu, K. Xu, H. Gu, R. Zheng, H. Liu, X. Zhang, Z. Guo and B. Xu, *J. Am. Chem. Soc.*, 2004, **126**, 9938–9939.
44 X. Gao, K. Tam, K. M. K. Yu and S. C. Tsang, *Small*, 2005, **1**, 949–952.
45 H. W. Gu, P. L. Ho, K. W. T. Tsang, C. W. Yu and B. Xu, *Chem. Commun.*, 2003, 1966–1967.
46 M. D. Shultz, J. U. Reveles, S. N. Khanna and E. E. Carpenter, *J. Am. Chem. Soc.*, 2007, **129**, 2482–2487.
47 D. Ma, J. Guan, F. Normandin, S. Denommee, G. Enright, T. Veres and B. Simard, *Chem. Mater.*, 2006, **18**, 1920–1927.